Demonstration of amplification of a polarized soft-x-ray laser beam in a neonlike germanium plasma

B. Rus,[1,2] C. L. S. Lewis,[3] G. F. Cairns,[3] P. Dhez,[1] P. Jaeglé,[1] M. H. Key,[4,5]
D. Neely,[4] A. G. MacPhee,[2] S. A. Ramsden,[6] C. G. Smith,[5] and A. Sureau[1]
[1]*Laboratoire de Spectroscopie Atomique et Ionique, URA 775 CNRS, Université Paris-Sud, Bâtiment 350, 91405 Orsay Cedex, France*
[2]*Department of Gas Lasers, Institute of Physics, CZ-18040 Prague 8, Czech Republic*
[3]*Department of Pure and Applied Physics, Queen's University of Belfast, Belfast BT7 1NN, United Kingdom*
[4]*Central Laser Facility, Rutherford Appleton Laboratory, Chilton, Oxon, OQ11 0QX, United Kingdom*
[5]*Clarendon Laboratory, University of Oxford, Oxford OX1 3PU, United Kingdom*
[6]*Department of Computational Physics, University of York, York YO1 5DD, United Kingdom*
(Received 8 August 1994)

We report results of polarization experiments on the collisionally excited Ne-like Ge soft-x-ray laser where we have used an injector-amplifier multistage geometry. The polarization state of the x-ray beam was analyzed by two crossed 45° angle of incidence multilayer mirrors which act as linear polarizers. Results were evaluated by comparing intensities of time-integrated beam patterns behind each polarizer. The polarization state of the amplified spontaneous emission (ASE) output at 23.2 and 23.6 nm from the injector plasma alone was systematically studied and, as expected, revealed no macroscopic degree of polarization observable within the precision of the experiment. When the injector output beam was linearly polarized by using a third 45° angle of incidence multilayer mirror and coupled into the amplifier plasma, the degree of polarization of the amplifier output was ~ 0.98, the total gain-length product attained for the polarized beam was ≈ 12, and the final beam energy was ≈ 20 nJ. The results obtained are discussed with relevance to processes determining the polarization properties of unsaturated ASE systems.

PACS number(s): 32.80.Wr, 42.55.−f, 42.50.Ar

I. INTRODUCTION

In recent years, worldwide soft-x-ray laser research has progressed to the point where many laboratories have routinely been able to produce simulated emission over a wide range of wavelengths [1,2]. While the search for new and more efficient routes to achieve x-ray lasing continues, there is a steady shift of current research effort in this field to control and hence to optimize various properties of the x-ray beam. Such studies include focusing the x-ray beam and improving its modal quality, divergence, and coherence properties [3–5]. One of the parameters of the x-ray laser beam, which may be of importance for a number of applications, is its polarization state. However, x-ray lasers operating in the amplified spontaneous emission (ASE) mode inherently provide unpolarized output. In a conventional laser, where light bounces back and forth in the laser cavity, polarization can be achieved due to an intracavity element allowing only one definite polarization to be above threshold for laser oscillations. Obviously, current x-ray lasers in either single- or double-pass configuration cannot exploit this approach in the usual sense and initial attempts have not claimed evidence for strongly polarized output [6].

A scenario promising to deliver partially polarized x-ray laser output by incorporating a whispering gallery mirror cavity [7] has been suggested. Here, amplification takes place in an active medium during several round-trips in the curved-surface cavity and the near grazing incidence reflections on the cavity wall would favor the electric vector parallel to it. To our knowledge, this approach has not yet been used experimentally, but would almost certainly require some form of synchronous pumping scheme.

Another and perhaps more straightforward approach to achieving polarized x-ray laser output consists of injecting an already polarized emission into an active medium and amplifying it to the desired intensity at the output. This approach has been exploited and successfully demonstrated in this work. It is clear that an alternative and less complicated approach is to simply polarize the unpolarized output from some combination of tandem amplifiers using a polarizer. However, this trivial approach limits the maximum achievable beam power to $\approx 15\%$ of the saturated output for the transition, assuming a polarizer with $\sim 30\%$ reflectance for *s*-polarized x rays; moreover, as seen later in this paper, the attainable degree of polarization would be rather low in this configuration if only one reflection on the polarizer is used.

Allowing for the fact that the experiment was carried out with time-integrated diagnostics, it had two primary objectives. The first was to verify that a simple nonsaturated amplified spontaneous emission is unpolarized, as concluded from the simple physical arguments presented below. The second was to demonstrate that a polarized x-ray beam can be amplified without significant degradation of its degree of polarization (or without suffering "depolarization"). This allows us to demonstrate that a linearly polarized x-ray laser beam of high

brightness can be delivered to meet the needs of polarization-specific applications.

The paper is organized in the following way. Section II outlines the processes determining the polarization state of unsaturated ASE systems and Sec. III evaluates the expected degree of polarization at an amplifier output. Section IV deals briefly with multilayer mirrors acting as polarizers in the soft-x-ray region and Sec. V describes the experimental configurations used in this work. Results obtained are presented in Sec. VI and discussed in Sec. VII with respect to the processes which might depolarize the x-ray beam during its amplification.

II. POLARIZATION PROPERTIES OF AMPLIFIED SPONTANEOUS EMISSION

In this regime, spontaneous emission produced somewhere in the active medium by excited ions is amplified along its trajectory by other excited ions and intense radiation emerges at the output. The spontaneous emission originates in vacuum fluctuations and since the individual emitting ions are virtually uncoupled (correlation might be expected only over a distance of the order of one wavelength), the orientations of their dipole moments as well as the phases of their dipole oscillations are uncorrelated. Starting from an uncorrelated source, a definite phase and orientation of the macroscopic electric field vector over the beam area gradually build up during the propagation of the emission in the medium. The phase (coherence) and polarization properties of the macroscopic radiation field are influenced by a number of processes taking place in the amplifying medium, such as collisions and the motion of the stimulated-emission producing ions. In other words, as for the longitudinal coherence, the polarization state of the ASE will not be determined merely by the properties of the source which triggered it, but will be associated with the character of the amplifying medium and the intensity of the ASE as well.

Although a number of theoretical papers have been devoted to related issues—for instance, a review of transverse coherence of ASE systems can be found in Ref. [8]—we are unaware of any work dealing explicitly with the macroscopic, time-dependent polarization properties of ASE. However, some papers treat various issues relevant to this problem, such as collisionally induced dephasing of the atomic polarization in the Maxwell-Bloch equations [9], the Maxwell-Bloch equations accounting for the individual M states of the lasing transition relevant to interaction with an arbitrarily polarized emission [10], and quantization of the field Hamiltonian in a paraxial approximation [11]. It is worth remarking that for superradiance systems, the polarization properties of the emitted light have been studied both experimentally [12] and theoretically [13]. Although not directly applicable to ASE systems, a good introduction to the topic of radiative transfer of polarized emission for astrophysical purposes may be found in [14]. In summary, there is an absence of references which would enable a straightforward analysis of this experiment and we will base the assessment of the ASE polarization features on its coherence parameters.

The fundamental interconnection of the coherence and polarization may be illustrated by considering collisions in the plasma. (The ion motion, leading to inhomogeneous Doppler broadening of the spectral line, is assumed to influence the polarization properties to a much lesser extent.) As the collisions randomly change the phase of the ion's dipole oscillations as well as orientation of its dipole moment, they will manifest themselves in both the macroscopic coherence and the polarization. Electron-ion elastic collisions occur so frequently in the relevant plasma conditions ($\nu_{ei} \approx 10^{14}$ s^{-1}) that within the lifetime of an excited ion against spontaneous or stimulated radiative decay ($\tau \approx 10^{-10}$ s for situations where saturation of the transition is not occurring) an ion will experience so many collisions that the phase and orientation of its dipole moment will be randomized. Indeed, the situation is more complex if we distinguish effects of long- and short-distance collisions. The latter, considerably shifting the energy levels and causing large disturbances of the oscillation phases, cause large orientation changes of the dipole moments. As a result, the spectral "wings" undergo larger variations of the polarization state than the line center does.

In the temporal coherence domain, collisional processes influence the spectral line shape in conjunction with other effects (ion motion, gain narrowing, etc). The coherence or phase of quasimonochromatic radiation of wavelength λ is maintained during the coherence time t_{coh} which may be evaluated via the spectral linewidth $\Delta\lambda$:

$$t_{\text{coh}} = \gamma \frac{\lambda^2}{c\Delta\lambda} , \tag{1}$$

where γ is a factor of order unity depending on the line profile ($\gamma = 0.32$, 0.66, and 1 for Lorentzian, Gaussian, and rectangular profiles, respectively) [15]. It is obvious that t_{coh} presents a useful estimate for the characteristic time during which a given polarization state of the macroscopic field is maintained, especially in the case where the contribution of collisions to the broadening of the spectral line is important.

Measurements of the $J=2 \rightarrow 1$ spectral line profile at 206.4 Å in Se [16] suggest that homogeneous broadening is significant. Taking $\Delta\lambda \sim 20$ mÅ as a linewidth estimate for ASE at $\lambda \approx 200$ Å under moderate gain-length product conditions, Eq. (1) gives $t_{\text{coh}} \approx 0.3$ ps. A typical x-ray laser pulse is hundreds of picoseconds in duration and will accordingly consist of perhaps several thousands of "wave trains," each with a definite polarization state. The polarization states of these wave trains are mutually uncorrelated and hence the emission is made up of a succession of randomly polarized "packets." Therefore, in the absence of a monitor with subpicosecond temporal resolution, the output of an unsaturated ASE x-ray laser should appear to be almost completely unpolarized.

Prior to closing this section, it should be emphasized that polarization is a local quantity. As a consequence, a rigorous description of ASE polarization must deal with the direction of polarization (or with the direction of the electric vector) over the emitted beam, as in the general case the polarization state is not uniform across the beam

front. Expansion of the beam field into transverse modes [8] may serve as an appropriate basis to illustrate this point. During the triggering of the ASE, different groups of atoms contribute to excite each of the modes to a different extent (this contribution is given by the scalar product of the triggering field distribution with the mode field distribution). As a result, different modes will have different polarization states. To obtain a uniform direction of polarization across the whole beam, a single-mode operation is necessary, or, equivalently, the Fresnel number $F=\pi a^2/(\lambda L)$ of the lasing medium ($2a$ is the width of the gain region and L the plasma length) must be close to one. This is indeed the same requirement as to achieve perfect transverse coherence and points again at the fundamental interconnection between the coherence and polarization. Concerning the experimental conditions, it follows that meaningful polarization measurements of an x-ray laser working in an ASE regime must be done in conditions close to single-mode operation.

III. AMPLIFICATION OF POLARIZED EMISSION

To quantify the polarization properties of an x-ray laser beam we will follow the conventional optical definition and define the degree of polarization D_p as [17]

$$D_p=\frac{I_p}{I_p+I_u}\ , \tag{2}$$

where I_p and I_u are the intensities of the polarized and unpolarized waves constituting the radiation of interest. We note that any quasimonochromatic beam can be represented as the sum of a polarized and an unpolarized component, where the two are independent.

The basic principle of the experimental arrangement which generates the polarized emission investigated in this work is illustrated in Fig. 1(a). A source (or injector) plasma of length l_s delivers an intense beam of completely unpolarized radiation (i.e., $D_p=0$) which is polarized by an x-ray optic having a total throughput efficiency R and then coupled into an amplifier plasma of length l_a with a coupling efficiency C. With the help of the Linford formula [18] the intensity emerging from the amplifier in the nonsaturated regime can be expressed as

$$I_{\rm amp}=RCw\frac{j_s}{g_s}\frac{\exp(g_s l_s+g_a l_a)}{\sqrt{g_s l_s+g_a l_a}}+w\frac{j_a}{g_a}\frac{\exp(g_a l_a)}{\sqrt{g_a l_a}}\ , \tag{3}$$

where j_s,g_s and j_a,g_a are peak spectral emissivities and gain coefficients of the source and amplifier plasmas, respectively. The factor $w=\sqrt{\pi\alpha\Delta\nu}$ treats the spectral line profile, where $\Delta\nu$ is the intrinsic frequency linewidth and α is a profile-dependent factor ranging from 0.5 for a Lorentzian to ~ 0.6 for a Gaussian. In deriving Eq. (3) it has been assumed that $\exp(g_s l_s)\gg 1$, $\exp(g_a l_a)\gg 1$, and that the spectral profiles for source and amplifier plasmas are identical.

The first term in Eq. (3) represents the emission from the source that is injected into and emergent from the amplifier, while the second term represents the normal ASE output from the amplifier itself. Assuming that ionization conditions are similar in each plasma so that $j_s\approx j_a$ and $g_s\approx g_a$ and that the plasma lengths are comparable, then to ensure that the first term dominates the output beam, we need to ensure that the condition $g_s l_s\gg\ln(RC)$ is satisfied.

Supposing that the emission injected into the amplifier maintains its polarization state during the amplification (the validity of this assumption will be discussed later), the degree of polarization of the first term in Eq. (3) will be identical to that of the emission entering the amplifier. On the other hand, the amplifier's own ASE contributes a

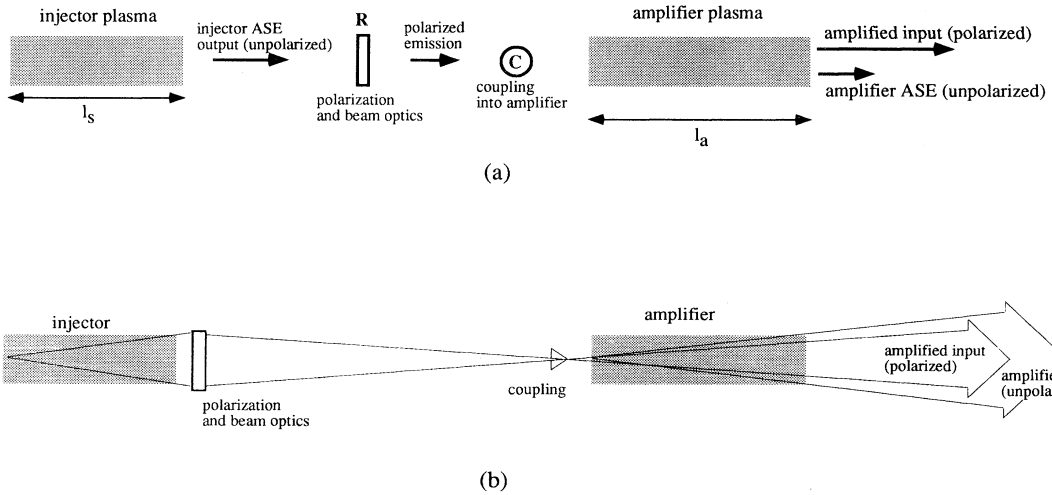

FIG. 1. (a) Generic scheme of an arrangement in which the ASE output from a source plasma is polarized by an optical device and subsequently amplified in another plasma. The efficiency of the polarizing and/or relaying x-ray optics is R and the coupling efficiency of the source emission into the amplifier gain region is C. (b) Generic sketch similar to that of (a), outlining schematically the divergence aspects of the x-ray emission generated in the studied system.

totally unpolarized signal to the output. Labeling the degree of polarization of the injected beam D_p^{in}, a straightforward application of Eqs. (2) and (3) yields an expression for the degree of polarization of the amplifier output D_p^{amp}

$$\frac{1}{D_p^{\text{amp}}}=\frac{1}{D_p^{\text{in}}}+\frac{j_a}{j_s}\frac{g_s}{g_a}\left[\frac{g_s l_s+g_a l_a}{g_a l_a}\right]^{1/2}$$

$$\times\exp[-g_s l_s-\ln(D_p^{\text{in}}RC)] \; . \qquad (4)$$

In the case $j_s\approx j_a$ and $g_s\approx g_a$, Eq. (4) reduces to $1/D_p^{\text{amp}}=1/D_p^{\text{in}}+\sqrt{(l_s+l_a)/l_a}\exp[-g_s l_s-\ln(D_p^{\text{in}}RC)]$. To ensure that the influence of the amplifier ASE on the output polarization is negligible, the second term on the right-hand side of Eq. (4) must be minimized. This requirement is met even for moderate values of $g_s l_s+\ln(D_p^{\text{in}}RC)$. In reality, however, there exist processes which are, during amplification, able to partially "depolarize" this already polarized emission. We will assess the magnitudes of some of these processes in a later section.

The actual experimental geometry clearly differs from the idealized scenario depicted in Fig. 1(a) and is subject to the details of beam propagation effects in the amplifiers. These include refraction and depolarization as well as the manner in which the beam is relayed and coupled, and these issues will be discussed later. Figure 1(b) indicates schematically some of the geometrical coupling effects possible.

IV. X-RAY POLARIZERS

The devices used in the present work to polarize and analyze the soft-x-ray lasing lines of interest at 23.2 and 23.6 nm were multilayer mirrors, each comprised of a stack of pairs of high- and low-Z materials and used at an angle of incidence of 45°. The ability of such a soft-x-ray mirror (XRM) to act as a polarizer is based on reflection at Brewster's angle at a sequence of dielectric interfaces [19]. Basically, such an x-ray polarizer is analogous to a pile-of-plates polarizer in visible optics and, as it is an interference mirror, there is an additional requirement for the thickness of one pair of layers to be approximately two-thirds of the operating wavelength for an incidence angle of 45°. The incidence angle must be close to 45° due to the fact that the real parts of the refractive indices are very close to unity at these wavelengths. Thus an s-polarized wave, having its electric vector parallel to the polarizer surface, is preferentially reflected. Although the reflectance of a p-polarized wave can be reduced by minimizing the surface roughness, it cannot be brought to zero as the materials used in the multilayer have a nonzero absorption (when reflection at Brewster's angle takes place at a dissipative medium, the p reflectivity is nonzero [17]). Thus to produce an efficient polarizer with the highest possible extinction ratio between s and p components requires careful design and consideration of the dissipative properties of the layer materials. It is also worth noting that compared to the normal incidence multilayer mirrors, only a few layer pairs are necessary here to reach high values of the reflectivity coefficient.

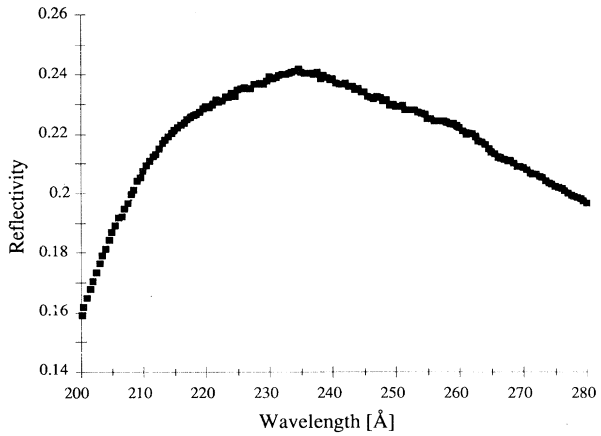

FIG. 2. Measured x-ray reflectivity versus wavelength for the Mo:Si polarizers used in this work, for s-polarized radiation incident under 45° [22].

The polarizers used in this work were coated onto 25-mm-diam superpolished, fused silica substrates with a rms surface roughness of less than 1 Å [20]. Three pairs of Mo:Si layers were produced by ion-beam sputtering [21] and the device properties were tested with synchrotron radiation [22]. As shown in Fig. 2, a reflectance of ~24% was achieved for s-polarized light at the design wavelength for a 45° incidence angle. Although the reflectance for p-polarized light was not measured on this occasion, calculations suggest [21] that the s-reflectance to p-reflectance ratio should be typically ~7.4, i.e., the p reflectivity being ~3.25%. These calculations also point at a fairly weak dependence of this ratio on the surface roughness (the ratio being 7.5 for an ideal roughness-free surface and 7.23 for a rms roughness of—unrealistically high—10 Å) as well as on other fabrication parameters. As the the degree of polarization depends on the measured data only by the s-reflectance to p-reflectance ratio, we have fair confidence in the results of our measurements.

If we know the intensity and polarization state of radiation incident on a polarizer with known reflectances R_s and R_p for s and p waves, then we can calculate the intensity and the polarization state of the radiation after reflection, using, e.g., Stokes vectors or Mueller matrix formalism [17]. We will consider several specific situations encountered in the present experiment and we assume $R_s > R_p$.

In the first case, a totally unpolarized beam of intensity I_{0u} is incident on the polarizer. The reflected beam will consist of an unpolarized component of intensity I_u and a linearly polarized component of intensity I_p, with its electric vector perpendicular to the plane of incidence. These intensities and the corresponding degree of polarization in the reflected beam are given by

$$I_p=\tfrac{1}{2}(R_s-R_p)I_{0u} \; , \qquad (5a)$$

$$I_u = R_p I_{0u} \ , \tag{5b}$$

$$D_p = \frac{R_s - R_p}{R_s + R_p} \ . \tag{5c}$$

In the second case, the partially polarized wave described by Eq. (5) is incident on a second and identical polarizer where the plane of incidence is also identical to the first case. After the second reflection the beam components are described as

$$I_p = \tfrac{1}{2}(R_s^2 - R_p^2) I_{0u} \ , \tag{6a}$$

$$I_u = R_p^2 I_{0u} \ , \tag{6b}$$

$$D_p = \frac{R_s^2 - R_p^2}{R_s^2 + R_p^2} \ . \tag{6c}$$

For the parameters of our polarizers, i.e., $R_s = 0.24 \pm 0.04$ and $R_p = 0.03 \pm 0.01$, Eq. (5) indicates that the degree of polarization achieved after a single reflection of an unpolarized beam is $D_p = 0.78^{+0.09}_{-0.11}$. After two reflections [Eq. (6)], the degree of polarization is improved significantly to $D_p = 0.97^{+0.02}_{-0.05}$.

The third relevant case is when a partially polarized beam with arbitrary degree of polarization is incident on the same polarizing element. If the polarized and unpolarized components have intensities I_{0p} and I_{0u}, respectively, then the total intensity reflected I_{out} depends on the direction of polarization of the polarized component. If the electric vector is perpendicular to the plane of incidence, then the corresponding output intensity is given by

$$I_{\text{out}} = R_s I_{0p} + \tfrac{1}{2}(R_s + R_p) I_{0u} \ . \tag{7a}$$

Alternatively, when the electric vector is parallel to the plane of incidence, the output intensity is given by

$$I_{\text{out}} = R_p I_{0p} + \tfrac{1}{2}(R_s + R_p) I_{0u} \ . \tag{7b}$$

These experiments will be exploited in the analysis of the amplifier beam polarization state in the regime of amplification of linearly polarized emission.

V. EXPERIMENTAL ARRANGEMENT

The experiment presented was carried out at the Central Laser Facility at the Rutherford Appleton Laboratory (RAL) [23,24]. The x-ray laser architecture available makes it possible to use x-ray optics to relay the x-ray laser beam from a source plasma and injection seed it into an additional, sequentially pumped distant plasma, acting as a final amplifier. The facility to manipulate the source beam before seeding it into the amplifier makes this setup suitable for a variety of experiments, one of them being the polarization study reported here.

The geometries of the experimental layouts used for the polarization studies are shown in Fig. 3. In Fig. 3(a) the set-up for a straightforward analysis of the polarization state of the ASE plasma output is shown. The north-going output is reflected from a near-normal incidence XRM (i.e., polarization insensitive) and returned along an axis which takes it close to, but not through, the source plasma. The beam polarization state is then analyzed using two crossed polarizers. In Fig. 3(b) the source ASE beam is linearly polarized to $D_p \sim 0.97$ by making it reflect twice off a 45° mirror polarizer before injection into the polarization analyzer system via an additional amplifier plasma. In the laboratory frame the injected beam is vertically polarized with the electric field parallel to the amplifier target surface. In each case the contribution from the south-going ASE output from the source plasma is eliminated by a carefully located beam-block.

The source plasma in each case was a double target amplifier which is now a routine configuration at RAL and consisted of two 22-mm-long, 100-μm-wide, and 0.6-μm-thick stripes of germanium coated onto glass substrates [5,23]. The targets were separated axially by 580 μm and laterally by 225 μm and each was irradiated, from opposite directions, by a group of three VULCAN laser beams. Each of these 110-mm-diam beams delivered ≈ 200 J of energy in ~ 650 ps full width at half maximum pulses at the fundamental wavelength of 1.06 μm. The net irradiance on each target was $\sim 1.6 \times 10^{13}$ W cm^{-2} with an expected gain coefficient on each of the $J = 2 \rightarrow 1$ lines at 23.2 and 23.6 nm of $\sim 3.5 \pm 0.5$ cm^{-1} [25]. We refer henceforth to this target as the "injector" plasma amplifier.

The normal incidence XRM used in each experiment was concave with a radius of curvature of 1 m. Its reflectance in the 23.2–23.6-nm spectral range was $\approx 10\%$. It was positioned 740 mm from the exit end of the injector and, for the second experiment, this corresponds to 1530 mm from the input end of the final amplifier plasma and we henceforth refer to this target as the "amplifier." The exit plane of the injector was image relayed to a plane ~ 60 mm in front of the amplifier input plane at an angle of ≈ 3 mrad and purposely offset ≈ 70 μm laterally from the amplifier surface to center on the expected position of the gain zone in the amplifier plasma. The amplifier was a 14-mm-long Ge stripe, otherwise similar to the injector components, and shot with a single VULCAN beam of 150 mm diameter. This beam delivered ≈ 400 J in ≈ 1 ns at 1.06 μm with a net irradiance of $\approx 1.3 \times 10^{13}$ W cm^{-2}. The amplifier was shot ≈ 7.55 ns after the injector to synchronize the injected beam with the gain phase in the amplifier. The expected gain coefficient in the amplifier plasma was estimated to be about 3.0 ± 0.5 cm^{-1} and hence the net amplification available was $\approx 70\times$.

We define the geometric coupling efficiency C as the fraction of the injector beam overlapping the gain region at the amplifier entrance plane. From earlier studies of these amplifiers it is known that the cross-sectional dimensions of the plasma gain region are ≈ 100 μm $\times \approx 75$ μm and that the typical beam divergence from the injector is ≈ 10 mrad, averaged over a polar distribution [23]. Allowing for the fact that we are image relaying with a magnification M of $\approx 2\times$ to a plane ~ 60 mm in front of the amplifier, the dimension of the x-ray laser beam at the amplifier entrance plane is comparable to the magnified injector output. The geometric coupling may be then assessed as $C \approx M^{-2}$ and here $C \approx 0.25$. The actual frac-

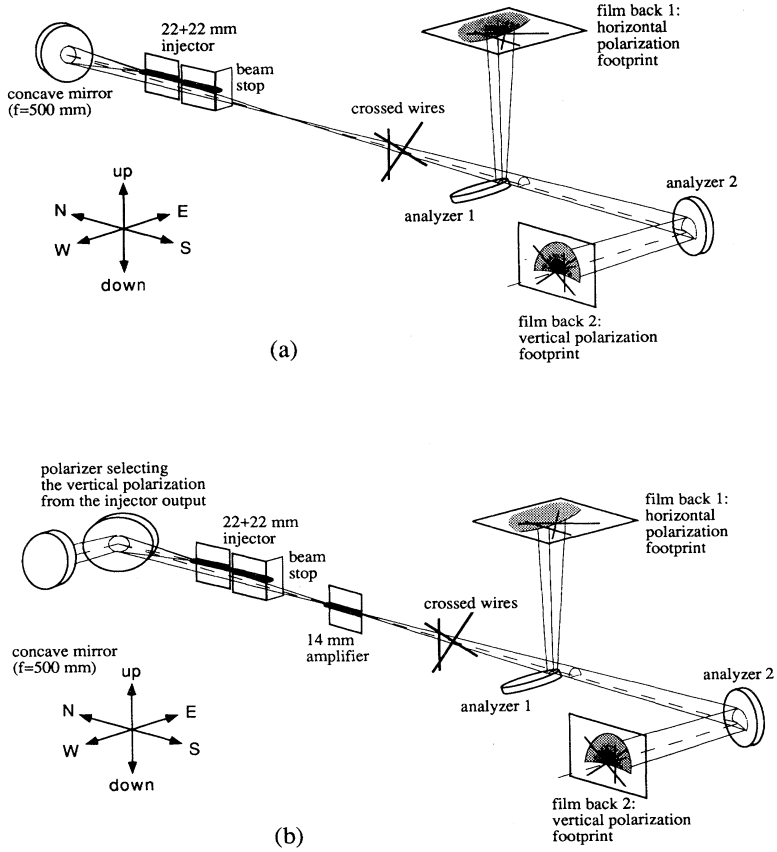

FIG. 3. (a) Experimental setup for the ASE injector output polarization state measurements (not to scale). The north-going injector output is relayed by a concave mirror. The first polarizer, reflecting chiefly the horizontally polarized emission, intercepts the bottom part of the x-ray beam and sends it toward the film back. The second polarizer, reflecting chiefly the vertically polarized emission, reflects the remainder of the beam and sends it toward the second film back. Any linearly macroscopically polarized light will yield different signals on the films (except for the case of light polarized in the direction of 45°). (b) Experimental setup for the amplification of the polarized emission measurements (not to scale). The north-going injector output is vertically polarized with $D_p = 0.97$ and relayed toward the amplifier; the injector exit face plane is imaged at a distance of ~ 60 mm in front of the amplifier entrance plane. The position of the crossed-wires system (placed 400 mm downstream from the amplifier output) as well as of the polarizers and film backs is the same as in (a).

tion of the injector beam entering the amplifier gain region is given by the product of this value with the throughput efficiency R of the x-ray optics. The intensity of the vertically polarized emission extracted from the injector beam by two reflections on the 45° mirror is given by Eq. (6a) and amounts to ~ 0.028 of the intensity leaving the concave mirror in the injector shots (we do not take into account the concave mirror as this is used in each experiment). The total coupling RC is then $\approx 0.25 \times 0.028 \approx 7 \times 10^{-3}$ so that $\approx \frac{1}{140}$ of the injector beam energy will be coupled into the amplifier, with an average divergence of ≈ 5 mrad. Not all this energy is expected to propagate and amplify through the full plasma length due to refraction and sensitivity to the injection angle, but regarding the accuracy of our knowledge of the parameters involved (degree of coupling, amplifier gain, and polarizer reflectivity), we can expect that the energy density at the detectors should not differ for shots with and without the final amplifier by more than a factor of about 3. Since this is well within the shot-to-shot reproducibility level of these high gain systems it is easily accommodated within the dynamic range of the detectors.

The beam emergent from the exit plane of the final amplifier was detected as a "footprint" on two film backs containing Kodak 104-02 soft-x-ray–sensitive film and protected from stray light by a 0.8-μm-thick aluminum filter. Each footprint involved reflection of the beam off a polarization analyzer element, but the distances from the amplifier exit plane to each film back were identical and equal to 1425 mm. We positioned a spatial fiducial in the beam at a distance of 385 mm from the amplifier exit plane. This consisted of three 150-μm-diam wires arranged in a triangular configuration and their shadows in the footprint patterns allowed us to align the images recorded in orthogonal states of linear polarization. Since we did not have a soft-x-ray beam splitter to analyze the whole beam in each of the two crossed analyzer

arms, we took advantage of the expected symmetry of the beam about the horizontal plane which bisects the stripe targets. To do this, we carefully arranged the first analyzer (which reflects horizontally polarized light) to intercept and reflect the lower half of the x-ray laser beam. The top half of the beam is transmitted past the edge of the polarizer and then analyzed for a vertically polarized component by the second, crossed analyzer. Using the fiducial wires, we were able to reconstruct the whole beam and make conclusions about the degree of polarization in the beam from the intensities recorded on each half of the reconstructed whole beam footprint.

VI. EXPERIMENTAL RESULTS

In the first part of the experiment, devoted to the injector ASE output polarization state measurements, 11 shots were fired with ±7% variance in drive intensity. Exposed films in each arm of the polarization analyzer were developed simultaneously after each shot. Images were densitometered with a Perkin Elmer PDS machine using 12-bit resolution and the digitized image transferred to a personal computer. Processing of the footprint images consisted of several steps. First, fog level optical density, which was recorded outside the shadow outline of the polarizers, was subtracted and the optical density above fog D converted to exposed radiation intensity I in units photons/μm^2 using the model equation $D=[1-\exp(-CI)]D_{\text{sat}}$, where the constants C and D_{sat} were taken from [26]. After correcting for filter transmittance and polarizer reflectance, the image was displayed as the actual flux in the x-ray laser beam. In a further step, a constant intensity value was subtracted from each image to allow for the exposure level recorded from plasma radiation within the mirror bandwidth,

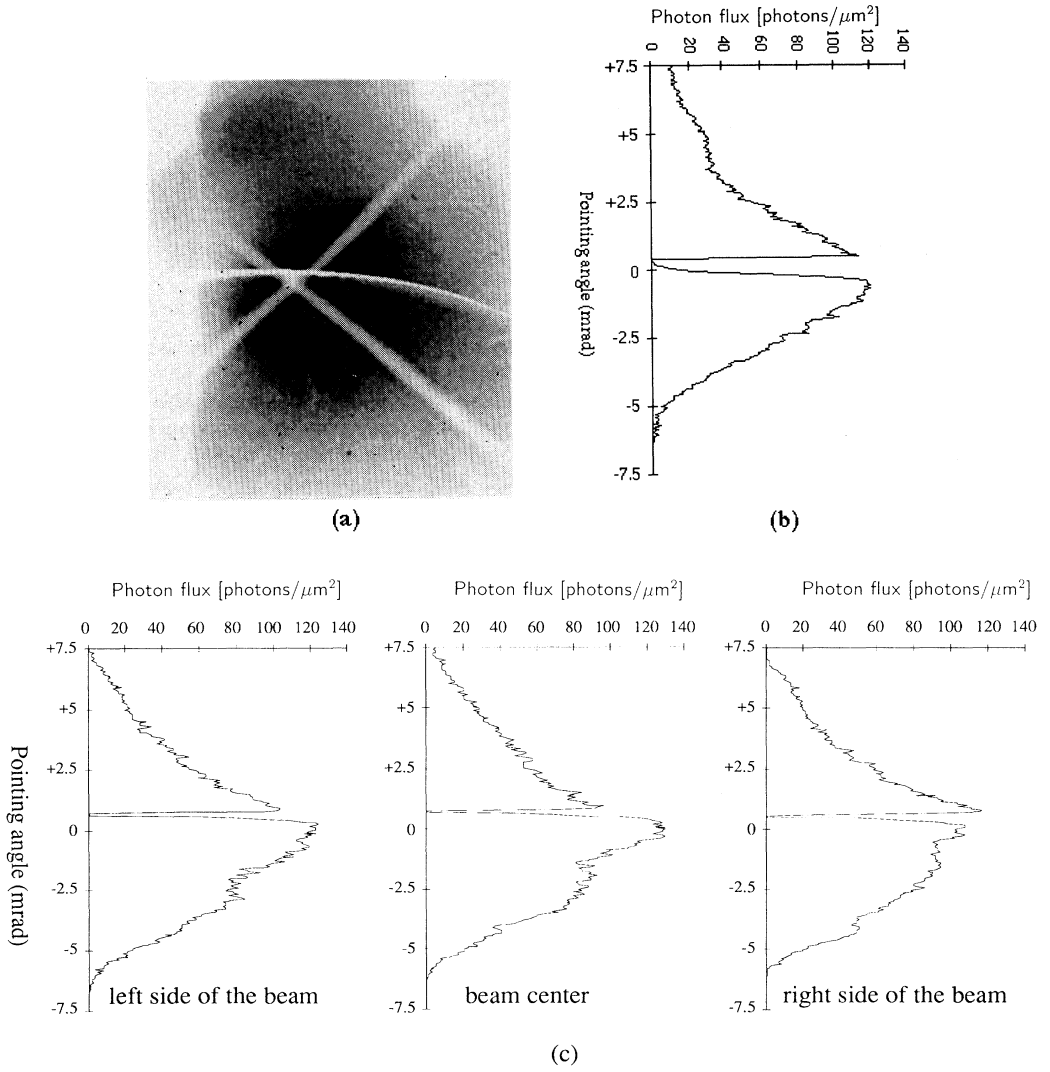

FIG. 4. (a) Composite footprint image of the injector output as viewed by the crossed polarizers. (b) Vertical densitometry trace of (a), passing through the crossed-wires center. The beam pointing angle is also measured relative to this center. (c) Vertical densitometry traces of a footprint from a shot where the crossed wires system was removed.

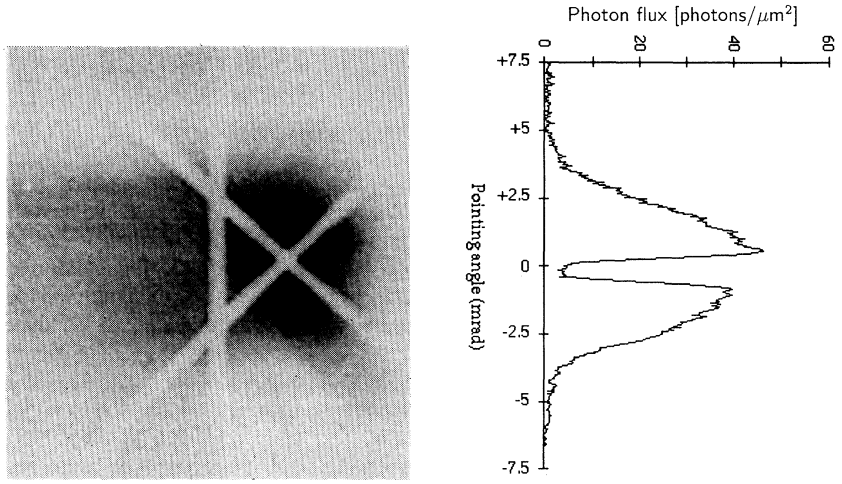

FIG. 5. (a) Footprint image of the amplifier output beam when the polarized emission is injected at the input, as viewed by the second polarizer (the first one is not mounted). (b) Vertical densitometry trace of (a), passing through the crossed-wires center.

which was measured on a null shot where there was no coupled beam and no footprint. In the final step, the two footprints from each shot were composed into a single image for further analysis.

A typical footprint image of the injector output beam is shown in Fig. 4(a), where the composite beam appears to have similar signal strength in each of the crossed polarizer arms. The position of the "center of gravity" of the beam relative to the first polarizer edge and to the spatial fiducial moved a little on a shot-to-shot basis making it inappropriate to exactly compare the top and bottom halves of the beam on all shots. Therefore we looked for intensity discontinuities across the joint in a composite image to signal the presence of macroscopic polarization in the beam. Examples of traces of beam intensity profiles taken vertically (in the laboratory frame) are shown in Figs. 4(b) and 4(c). The dip near the center of Fig. 4(b) corresponds to both the wire fiducial and the image joint and relates to Fig. 4(a). Some shots were taken without the wire fiducial and an example is shown in Fig. 4(c), where several parallel vertical scans are presented, with the dip now due solely to the image joint. Any intensity discontinuities are averaged over several of such traces in a given shot.

From the data thus collected we conclude that neither the upper nor the lower half of the footprints is systematically more intense, which means that under the injector conditions there is no preferred, systematic direction of polarization in the x-ray beam. Within the accuracy of the experiment, estimated to be $\approx 5\%$, the time-integrated degree of polarization is zero.

In the second part of the experiment, where amplification of polarized light was studied, eight shots were taken. In addition, one comparative shot was fired where the injector beam was relayed directly to the amplifier without being polarized. In all cases whole-beam footprint images were reconstructed as before.

The high quality of the amplified beam profile is shown in Fig. 5, where for the purpose of illustrating this point the first analyzer was removed from the beam path, allowing the second analyzer to reflect the vertically polarized component of the whole beam. A typical result with

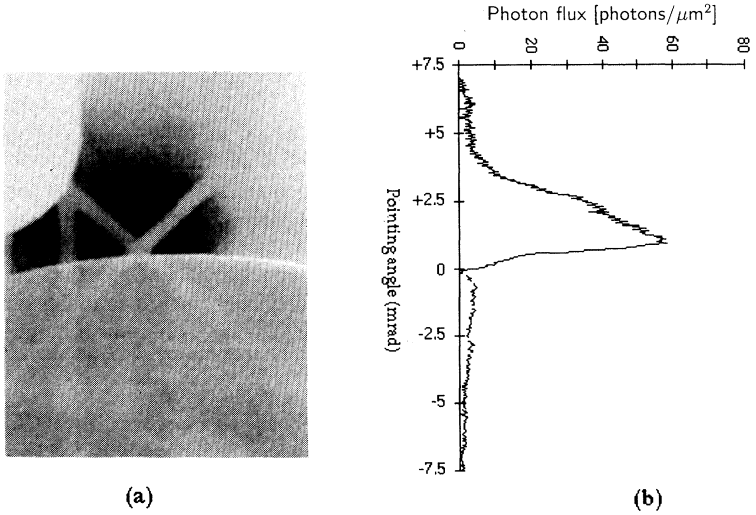

FIG. 6. (a) Composite footprint image of the amplifier output beam when the polarized emission is injected at the input. (b) Vertical densitometry trace of (a), passing through the crossed-wires center.

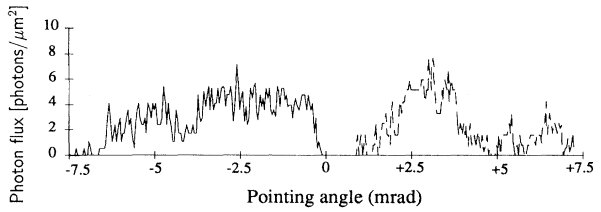

FIG. 7. Densitometry trace of the amplifier output when no emission is injected at the input. The shot was performed at a high energy of the driving laser (470 J).

both analyzers in place is shown in Fig. 6. Here we see that the bottom half of the beam, analyzed for a horizontal polarization, contains virtually no signal, which indicates a high degree of vertical polarization of the amplified beam.

Quantitative analysis of the image intensities, allowing us to solve for the polarized and unpolarized intensity components contained in the beam and hence for the degree of polarization of the amplified beam, is carried out with the help of Eq. (7). Averaging over the performed shots we find $D_p = 0.98^{+0.02}_{-0.05}$, which is essentially the same value as the degree of polarization of the injected beam. This means that within the precision of the experiment and under its conditions (i.e., total effective gain-length product for the vertically polarized light ≈ 12, of which ≈ 4 exponential foldings are associated with the final amplifier) there is no depolarization of the amplifying beam. To support these conclusions the experiment was completed by some null shots. In Fig. 7 we see a densitometric trace of the footprint recording ASE signal levels (approximately zero) when only the final amplifier is fired. Figure 8 displays a densitometric trace of the footprint from the shot where an unpolarized injector signal is relayed to the amplifier. Although the center of gravity is slightly shifted in the vertical direction with respect to the first analyzer edge, it is evident that the amplified beam is unpolarized.

Finally, from absolute calibration data of the film used, we estimate that the polarized beam x-ray laser delivered

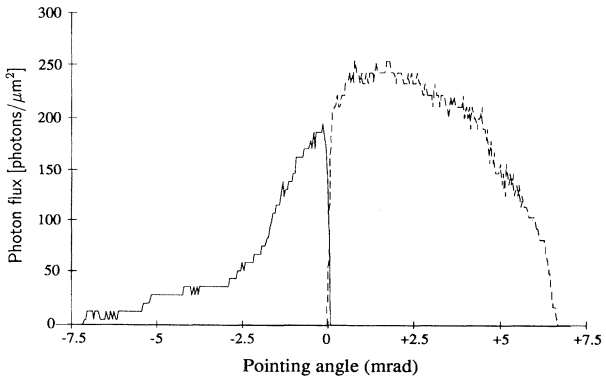

FIG. 8. Densitometry of the amplifier output footprint from the shot in which an unpolarized beam was injected at the amplifier input.

≈ 20 nJ of energy in this particular experiment. This should scale to the millijoule level under saturated output conditions.

VII. DISCUSSION

The results obtained in the first part of this work verify the basic validity of the given picture about ASE polarization properties. It is clear that the injector output beam was unpolarized within the limits of precision of the experiment: from Fig. 4(c) it is quite obvious that the small jumps between the signal of the upper and lower footprints may well be caused either by noise or by diffraction on the polarizer edges. This fact, together with the lack of a sufficient number of identical shots, limits here the use of a statistical method developed for deducing even an extremely weak macroscopic degree of polarization of the x-ray laser beam [27] (supposing that the time-integrated direction of polarization changes randomly from shot to shot). Two other aspects of the performed experiment should be emphasized. First, due to the relatively large bandpass of the polarizers used, the footprints contain signals from both lasing transitions at 23.2 and 23.6 nm. We thus have an "overlap" of two beams whose polarization states are mutually uncorrelated (both the upper and lower lasing levels of these transitions are different); this even lessens the resulting degree of polarization of the whole x-ray laser beam. Second, the Fresnel number of the injector ($22+22+0.58$ mm long) is ~ 4 in the horizontal plane and ~ 16 in the vertical plane, assuming that the gain region has a horizontal dimension of ~ 75 μm and a vertical dimension of ~ 150 μm. These are satisfactory numbers, although we are still far from a single-mode operating ASE.

The central point of the results obtained when the injector output was linearly polarized and amplified is the observation that no detectable change of the polarization state took place during the process of amplification. In general, there are three possible processes able to depolarize the emission propagating down the below-saturation threshold amplifying medium: (i) the amplifier proper—and unpolarized—ASE, (ii) the Faraday rotation of the electric vector of the x-ray beam in the spontaneous magnetic field produced in the plasma, and (iii) collisions experienced by the amplifying ions, changing the orientation of their dipole moments.

Concerning the contribution of the ASE to the total amplifier output, it can be evaluated using Eq. (3). Taking D_p^{in} of the injected beam as 0.97, $g_s = 3.5$ cm^{-1}, $l_s = 4.4$ cm, $g_a = 3.0$ cm^{-1}, $l_a = 1.4$ cm, and $RC = 7 \times 10^{-4}$ (accounting now for the throughput of all the x-ray optic elements used) and assuming that the emissivities of the injector and the amplifier are the same, we find that the degree of polarization of the amplifier output is essentially unchanged with $D_p^{\text{amp}} \sim 0.97$. This indicates that any small changes expected will not be detected within our experimental precision.

Under the presence of a magnetic field, the amplifying plasma behaves as a magnetoactive medium and, as a result, the polarization state of the x-ray laser beam will undergo changes. In the laser-plasma interaction conditions

relevant to x-ray lasers, the dominant source term of the spontaneously generated magnetic fields will be the effect of noncollinear gradients of the electron temperature and density. The magnitude of magnetic fields generated in this way may be estimated as [28] $\mathbf{B} \approx (k \nabla T_e \times \nabla n_e)/(q n_e |\nabla u|)$, where T_e and n_e are, respectively, the electron temperature and the density, q is the electronic charge, and u is the plasma macroscopic flow velocity. As the density gradient is largest in the direction perpendicular to the target surface and the temperature gradient component is predominantly in the lateral direction, the magnetic field $\mathbf{B}$ will be parallel to the plasma axis and hence to the propagation direction of the x-ray laser. Under these conditions, the Faraday effect must be considered, i.e., a linearly polarized electromagnetic wave propagating in a plasma along the applied magnetic field will rotate its direction of polarization. Considering the geometry according to Fig. 3(b), the B field is directed downstream from the x-ray beam propagation in the upper part of the amplifier plasma and counterstream in the lower part. In the upper plasma region where the x-ray beam propagates parallel to the magnetic field, the wave E vector will be rotated counterclockwise (viewed downstream from the x-ray beam propagation), and in the bottom plasma region where the beam propagation direction and the magnetic field are antiparallel, it will be rotated clockwise. The amplifier plasma thus does not act analogously to a conventional Faraday rotator, but instead tends to bend the E field lines, as shown in Fig. 9. As the magnitude of the magnetic field fluctuates, the whole mechanism has the potential to depolarize an initially linearly polarized x-ray beam.

To estimate the amplitude of the magnetic field in the gain region, we take [29] $n_e \sim 3 \times 10^{20}$ cm^{-3}, $\nabla n_e \sim 2 \times 20^{23}$ cm^{-4}, $\nabla T_e \sim 1 \times 10^4$ eV/cm (assuming that the expansion is approximately cylindrical), and $\nabla u \sim 3 \times 10^9$ s^{-1} [30]; we thus obtain $B \approx 20$ T. The plane of polarization of an emission propagating along the magnetic field over a distance l_a will turn by an angle given approximately by [31]

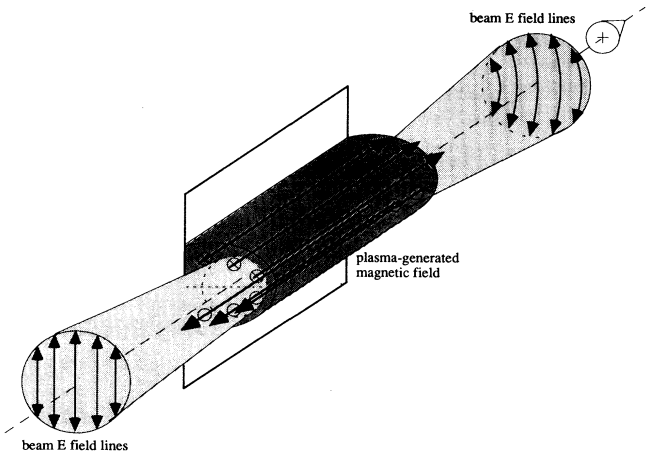

FIG. 9. Schematic of self-generated magnetic field in an x-ray laser plasma amplifier: its effect on a vertically polarized emission injected at the amplifier's input is also shown.

$$\Phi \approx \frac{n_e}{n_{\rm cr}} \frac{qB}{2m_e c} l_a \ , \tag{8}$$

where $n_{\rm cr}$ is the critical electron density for the wave undergoing the Faraday rotation ($n_{\rm cr} \sim 2 \times 10^{24}$ cm^{-3} for 23.6 nm) and m_e the electron mass. For $l_a = 1.4$ cm, we obtain $\Phi \sim 12.4$ mrad, i.e., $\sim 0.7°$. We may therefore conclude that the effect of the spontaneously plasma-generated magnetic fields on the polarization state of the x-ray laser beam is negligible under the experimental conditions encountered. However, the whole mechanism might be of importance for high-brightness, short driving pulses and/or for small-lateral-dimension plasmas, where additional processes may create larger magnetic fields.

For the third source of possible depolarization—the effect of collisions experienced by the amplifying ions—no quantitative assessment is available. However, the short-distance collisions which have the strongest depolarizing effect influence predominantly the wings of the spectral profile, where gain is marginal. In addition, the amplification further reduces the spectral width of the lasing line by gain-narrowing effects and therefore the emission whose polarization state was collisionally changed will not be effectively amplified. As a result, the overall depolarization due to the collisions in the amplifying plasma is expected to be small. This claim seems to be evidenced experimentally in this work as no observable depolarization of the amplifier beam was detected.

VIII. CONCLUSIONS

In summary, the polarization state of two $J = 2 \rightarrow 1$ lasing lines at 23.2 and 23.6 nm in a neonlike Ge soft-x-ray laser has been investigated in two different experimental arrangements. Whereas in the first setup we studied natural polarization properties of an ASE x-ray laser output, the amplification of the linearly polarized beam was examined in the second part of this work. For both these cases we have presented rather simple background arguments, making it possible to estimate the importance of the processes influencing polarization properties of the x-ray beam. These arguments suggest, taking the longitudinal coherence time as an estimate, that one definite polarization state in a below-saturation ASE regime lasts a fraction of a picosecond. The consequent expectation that a typical ASE output should appear virtually unpolarized in time-integrated diagnostics was confirmed experimentally. The injector beam was observed neither to be preferentially polarized in any direction nor to show a measurable degree of polarization.

The second experimental arrangement was designed to actively control the polarization state of the x-ray beam produced by an injector-amplifier scheme. To that end, only vertical polarization was selected from the injector beam prior to feeding it into the amplifier plasma. The measured degree of polarization $D_p \sim 0.98$ of the amplifier output beam has been found to be identical (within the experimental precision) to the degree of polarization of the injected beam. This result is consistent with the basic arguments suggesting that the depolarization effects should be fairly weak.

Producing a highly polarized x-ray beam of a good spatial quality is the major achievement of this work. The relatively low beam energy achieved here (with an effective gain-length product of ≈ 12) can in principle be increased to saturation level (millijoule) by the addition of further synchronized amplifiers.

Numerous applications of polarized x-ray laser beam have been anticipated in the literature; let us briefly mention at least some of them. Polarized x-ray emission is of concern in interferometry and holography [32], where the highest contrast of fringes is produced for the polarization perpendicular to the plane formed by the propagation vectors of the interfering beams. Polarization is an important parameter in those interactions of the soft-x-ray radiation with atomic, molecular, or solid-state systems where anisotropy of the studied process exists. A number of applications of polarized x-ray lasers in this field are reviewed in Refs. [33–35]; they include topics of investigation such as inner-shell photoionization, stimulated radiative recombination, surface or interface physics by photoelectron spectroscopy, dynamics of molecular photofragmentation, etc. Another technique requiring linearly polarized soft-x-ray emission is x-ray dichroism microscopy [36], where near-edge x-ray absorption is used in studying orientational characteristics of specific chemical bonds. Finally, another important field of applications of polarized x-ray lasers is the proposed soft-x-ray nonlinear optics such as four-wave mixing [37], where collinearity of the electric vectors of the involved x-ray laser and the visible laser is required.

ACKNOWLEDGMENTS

The authors are pleased to acknowledge the excellent work of J. M. Chauvineau and his team from the Institut d'Optique in Orsay, who designed and fabricated the multilayer polarizers. We would further like to thank T. Lucatorto, C. Tarrio, and R. Watts of the NIST Physics Laboratory, Gaithersburg, for the reflectivity tests of these polarizers. We are also indebted to A. Klisnick and P. Zeitoun of LSAI for their kind help in the film densitometry and to Phil Holden for a number of useful discussions. Finally, we thank the VULCAN laser and target area staff who ensured the success of this collaborative project.

[1] C. J. Keane, Proc. Soc. Photo-Opt. Instrum. Eng. **1551**, 2 (1991).

[2] D. L. Matthews, in *X-Ray Lasers 1992,* edited by E. E. Fill, IOP Conf. Proc. No. 125 (Institute of Physics and Physical Society, Bristol, 1992), pp. 31–35.

[3] *Applications of X-ray Lasers,* edited by R. London, D. Matthews, and S. Suckewer, Proceedings of the Workshop, San Francisco, 1992, National Technical Information Service Document No. LLNL-CONF-9206170.

[4] J. Trebes, in *X-Ray Lasers 1992* (Ref. [2]), pp. 265–268.

[5] C. L. S. Lewis, D. Neely, D. O'Neill, J. Uhomoibhi, G. Cairns, A. MacPhee, G. J. Tallents, J. Krishnan, L. Dwivedi, M. H. Key, P. Norreys, R. Kodama, R. E. Burge, G. Slark, M. Brown, G. J. Pert, P. Holden, M. Lightbody, S. A. Ramsden, J. Zhang, C. Smith, P. Jaeglé, G. Jamelot, A. Carillon, A. Klisnick, J. P. Raucourt, J. E. Trebes, M. R. Carter, S. Mrowka, and K. A. Nugent, in *X-Ray Lasers 1992* (Ref. [2]), pp. 23–30.

[6] K. Murai, G. Yuan, R. Kodama, H. Daido, Y. Kato, M. Niibe, A. Miyake, M. Tsukamoto, Y. Fukuda, D. Neely, and A. MacPhee, Jpn. J. Appl. Phys. (to be published).

[7] M. H. Muendel and P. L. Hagelstein, in *Femtosecond to Nanosecond High-Intensity Lasers and Applications,* edited by E. M. Campbell, SPIE Proc. 1229 (SPIE, Bellingham, WA, 1990), pp. 87–96.

[8] R. A. London, Phys. Fluids B **5**, 2707 (1993).

[9] G. Hazak and A. Bar-Shalom, Phys. Rev. A **38**, 1300 (1988).

[10] A. Sureau, in *X-Ray Lasers 1992* (Ref. [2]), pp. 251–254; also see A. Sureau and B. Rus (unpublished).

[11] J. C. Garrison, H. Nathel, and R. Y. Chiao, J. Opt. Soc. Am. B **5**, 1528 (1988).

[12] A. Crubellier, S. Liberman, P. Pillet, and M. G. Schweighofer, J. Phys. B **14**, L177 (1981).

[13] A. Crubellier, S. Liberman, and P. Pillet, J. Phys. B **19**, 2959 (1986).

[14] D. Rees, in *Numerical Radiative Transfer,* edited by W. Kalkofen (Cambridge University Press, Cambridge 1987), and references cited therein.

[15] J. W. Goodman, *Statistical Optics* (Wiley, New York, 1985), Chap. 5.

[16] J. A. Koch, B. J. MacGowan, L. B. DaSilva, D. L. Matthews, J. H. Underwood, P. J. Batson, and S. Mrowka, Phys. Rev. Lett. **68**, 3291 (1992).

[17] See, e.g., M. Born and E. Wolf, *Principles of Optics* (Pergamon, Oxford, 1985).

[18] G. J. Linford, E. R. Peressini, W. R. Sooy, and M. L. Spaeth, Appl. Opt. **13**, 379 (1974).

[19] P. Dhez, Nucl. Instrum Methods Phys. Res. A **261**, 71 (1987).

[20] Specifications provided by the substrate fabricator General Optics, Inc., 554 Flinn Avenue, Moorpark, CA 93021.

[21] J. P. Chauvineau (private communication).

[22] The reflectivity tests were performed at NIST Physics Laboratory, Physics Bldg., Rm. B160, Gaithersburg, MD 20899.

[23] G. Cairns, C. L. S. Lewis, A. G. MacPhee, D. Neely, M. Holden, J. Krishnan, G. J. Tallents, M. H. Key, P. N. Norreys, C. G. Smith, J. Zhang, P. B. Holden, G. J. Pert, J. Plowes, and S. A. Ramsden, Appl. Phys. B **58**, 51 (1994).

[24] G. F. Cairns, D. M. O'Neill, C. L. S. Lewis, D. Neely, A. G. MacPhee, C. Danson, A. Damerell, M. H. Key, D. Rodkiss, and R. Wyatt, Rutherford Appleton Laboratory Annual Report No. RAL-93-031, 1993 (unpublished).

[25] D. Neely, C. L. S. Lewis, D. M. O'Neill, J. O. Uhomoibhi, M. H. Key, S. J. Rose, G. J. Tallents, and S. A. Ramsden, Opt. Commun. **87**, 231 (1992).

[26] J. Krishnan, D. Neely, C. Danson, L. Dwivedi, C. L. S.

Lewis, and G. J. Tallents, Rutherford Appleton Laboratory Annual Report No. RAL-92-020, 1992 (unpublished).
[27] B. Rus, Ph.D. thesis, Laboratoire de Spectroscopie Atomique et Ionique, Université Paris-Sud, 1995.
[28] W. L. Kruer, *The Physics of Laser Plasma Interactions* (Addison-Wesley, Redwood City, CA, 1988), Chap. 12.
[29] P. B. Holden, S. B. Healy, M. T. M. Lightbody, G. J. Pert, J. A. Plowes, A. E. Kingston, E. Robertson, C. L. S. Lewis, and D. Neely, J. Phys. B **27**, 341 (1994).
[30] G. J. Pert, in *X-Ray Lasers 1990,* edited by G. J. Tallents, IOP Conf. Proc. No. 116 (Institute of Physics and Physical Society, Bristol, 1991), pp. 143–150.
[31] J. A. Stamper, Laser Part. Beams **9**, 841 (1991).
[32] See, e.g., R. J. Collier, C. B. Burckhardt, and L. H. Lin, *Optical Holography* (Academic, Orlando, 1971), Chap. 7.
[33] B. Crasemann, in *Applications of X-ray Lasers* (Ref. [3]), pp. 67–89.
[34] R. D. Deslattes, in *Applications of X-ray Lasers* (Ref. [3]), pp. 109–122.
[35] G. D. Kubiak, in *Applications of X-ray Lasers* (Ref. [3]), pp. 134–140.
[36] H. Ade and B. Hsiao, Science **262**, 1427 (1993).
[37] M. H. Muendel and P. L. Hagelstein, Phys. Rev. A **44**, 7573 (1991).

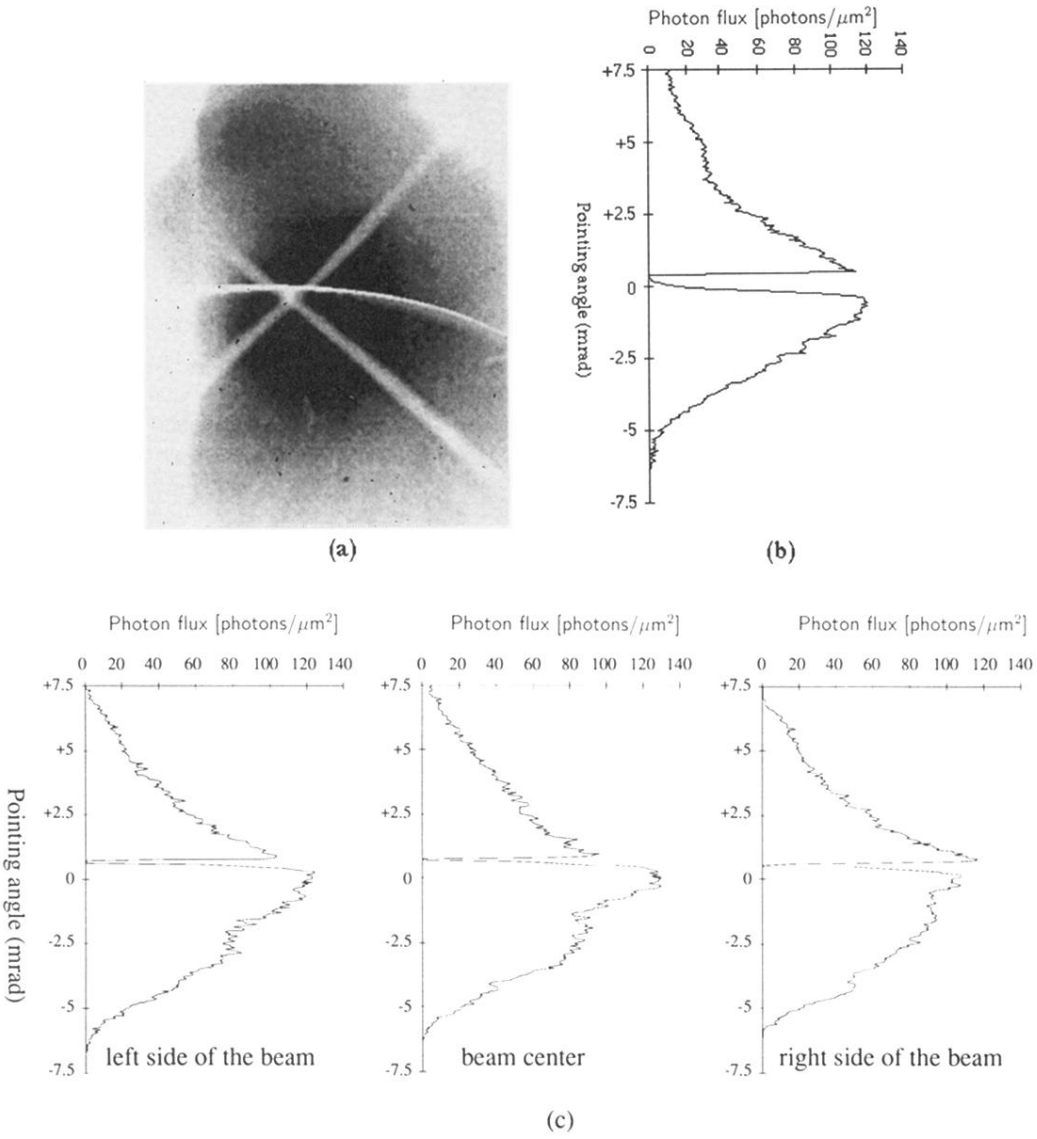

FIG. 4. (a) Composite footprint image of the injector output as viewed by the crossed polarizers. (b) Vertical densitometry trace of (a), passing through the crossed-wires center. The beam pointing angle is also measured relative to this center. (c) Vertical densitometry traces of a footprint from a shot where the crossed wires system was removed.

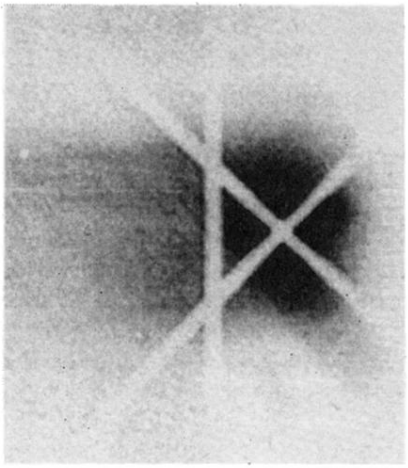

(a)

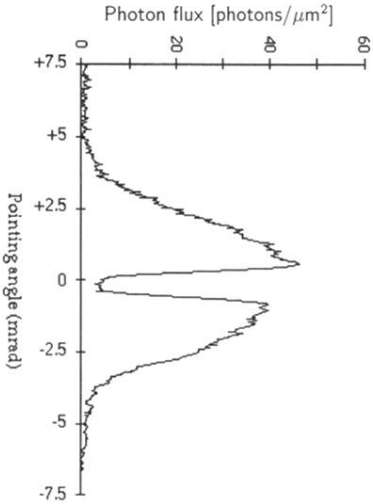

(b)

FIG. 5. (a) Footprint image of the amplifier output beam when the polarized emission is injected at the input, as viewed by the second polarizer (the first one is not mounted). (b) Vertical densitometry trace of (a), passing through the crossed-wires center.

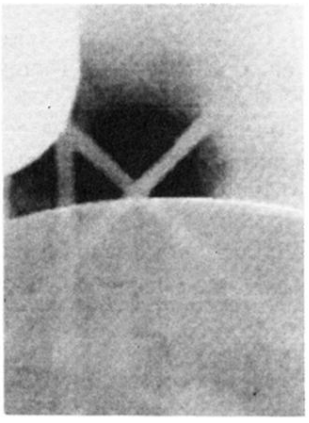

(a)

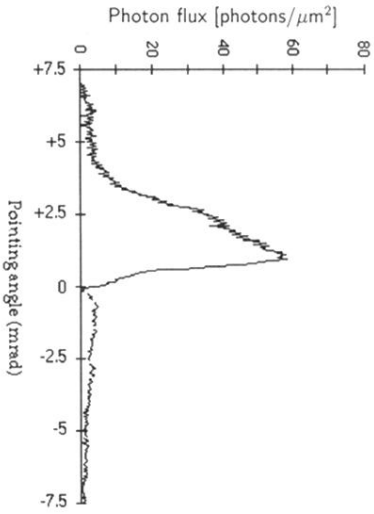

(b)

FIG. 6. (a) Composite footprint image of the amplifier output beam when the polarized emission is injected at the input. (b) Vertical densitometry trace of (a), passing through the crossed-wires center.